

We are IntechOpen, the world's leading publisher of Open Access books Built by scientists, for scientists

6,900

Open access books available

186,000

International authors and editors

200M

Downloads

Our authors are among the

154

Countries delivered to

TOP 1%

most cited scientists

12.2%

Contributors from top 500 universities



WEB OF SCIENCE™

Selection of our books indexed in the Book Citation Index
in Web of Science™ Core Collection (BKCI)

Interested in publishing with us?
Contact book.department@intechopen.com

Numbers displayed above are based on latest data collected.
For more information visit www.intechopen.com



Application of Scanning Acoustic Microscopy to Pathological Diagnosis

Katsutoshi Miura

Additional information is available at the end of the chapter

<http://dx.doi.org/10.5772/63405>

Abstract

Scanning acoustic microscopy (SAM) can obtain high-quality microscopic images of tissues and cells that are comparable with light microscopic images without staining and within only a few minutes. The speed of sound through tissues and cells is correlated with elasticity, thereby indicating their biomechanical properties. The elasticity varies according to the contents, such as collagen or elastic fibers, blood, colloids, mucin, ground substances, and cytoskeleton; therefore, SAM can follow changes in the composition of tissues and cells to determine their functions. Chemical modifications such as fixation, periodic acid-Schiff reaction, and enzymatic digestion may influence acoustic properties, and SAM can follow these changes over time in the same section to facilitate statistical comparisons based on digital values. Digital imaging using SAM is superior to analog methods for modifying images to discriminate changes, such as malignant and benign cell types. The observation ranges are shown in a colored column, and they can be manually adjusted. Thus, precise differences in acoustic properties are readily distinguished by narrowing the range. The resolution of SAM is determined by the wavelength, and it can theoretically exceed that of visible light. Combining these distinct techniques may help to elucidate the structural and functional characteristics of tissues and cells.

Keywords: elasticity, histochemistry, imaging analysis, protease, scanning acoustic microscopy

1. Introduction

Sound travels through different human body tissues at specific speed of sound (SOS) values. Harder materials have greater SOS values; thus, the SOS through each tissue can provide

information regarding its elasticity. Scanning acoustic microscopy (SAM) can be used to calculate the SOS, the attenuation of sound (AOS), and the thickness of tissues, before plotting the data on the screen to form images (**Figure 1**). SAM was first developed in the early 1970s by Lemons and Quate at Stanford University (CA, USA) [1], and the basic design is now used in the biomedical area. In SAM, the image contrast depends on the biomechanical properties of the tissues and the frequency and focusing conditions [2]. In general, sections that contain little structural protein possess SOS and AOS values that are similar to water in the coupling medium. By contrast, sections containing structural proteins such as collagens have significantly greater SOS and AOS values than water.

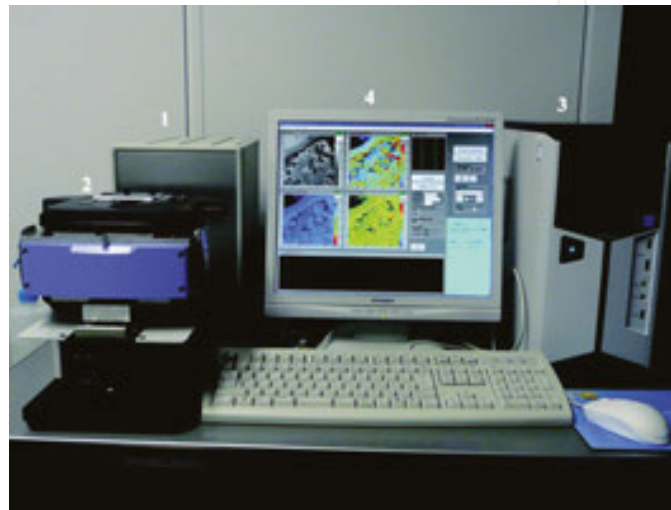


Figure 1. Appearance of scanning acoustic microscope systems. 1. Signal processor, 2. mechanical scanner with transducer, 3. system control PC, and 4. display.

In previous studies, we have observed various organs, such as the lung [3], gastrointestinal tract [4], thyroid [5], liver [6], heart [6], blood vessels [6], skin [6], and lymph nodes [7], where we used tissue sections and cytological specimens [8]. In further applications, we followed histological changes over time after chemical modifications such as fixation, staining, and digestion [6], where we compared the fresh unfixed sections with formalin-fixed sections. We employed SAM to observe the histological changes following the periodic acid-Schiff (PAS) reaction. After protease digestion, the SAM images were followed over time to examine the sensitivity or resistance to enzymatic treatment.

In this mini review, we explain the SAM system in the following order: principle of SAM, preparation of sample materials, observation procedure, application of SAM to tissue and cytology diagnosis, differentiation between malignant and benign, fixation effects, effects of PAS reaction, effects of collagenase, statistical analysis, and conclusion.

2. Principles of acoustic microscopy

The basic design of a reflective scanning acoustic microscope is shown in **Figure 2**.

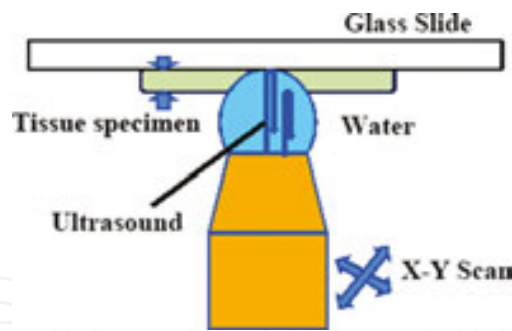


Figure 2. Principle of SAMs. Ultrasonic waves from the transducer reflect off both the glass slide and the sample section before returning to the transducer. The waves pass through 10- μ m sample sections with different ultrasonic properties. The transducer automatically scans the section to calculate the speed of sound (SOS) through each area. The section is placed upside down on the transducer, and distilled water is applied between the transducer and the section as a coupling fluid. The control SOS through water is 1495 m/s.

A piezoelectric transducer converts a radio frequency signal into an acoustic wave, which is then focused by a sapphire lens onto the glass slide where the histology specimens are mounted. A coupling liquid (usually water) carries the sound wave between the lens and the specimen. The beam is focused on the slide at a fixed distance from the lens. Components of the acoustic wave may be reflected, scattered, absorbed, or transmitted, which is determined primarily by the elastic properties of the tissue. The waves reflected from both the glass slide and the specimens are then collected by the same lens. The intensity of the resulting acoustic signal is then converted into brightness for display purposes. The specimen is scanned in the horizontal plane in a raster fashion to allow point-by-point analysis of the elastic properties of a cross-section of tissue [9].

The SAM can be used as basic data to assess the biomechanics of tissues and cells. The relationship between the SOS and the elastic bulk modulus of a liquid-like medium is given by the Newton-Laplace equation as follows:

$$c = \sqrt{K / \rho}, \quad (1)$$

where c is the SOS, K is the elastic bulk modulus, and ρ is the density.

Thus, the SOS increases with the stiffness (the resistance of an elastic body to deformation by an applied force) of the material, whereas it decreases with the density. Excluding bones (1.750 g/cm³) and fats (0.9094 g/cm³), the average soft tissue density is almost 1 g/cm³, which is the same as water (<http://www.scrollseek.com/training/densitiesofdifferentbodymatter.html>), and the SOS through soft tissues is strongly correlated with their hardness.

Recent biomechanical studies suggest that the mechanical properties of tissues might not be sufficiently similar to liquids, and thus they should be treated as soft solid materials. The sound waves that generate volumetric deformations (compression) and shear deformations (shearing) are called pressure waves (longitudinal waves) and shear waves (transverse waves), respectively.

The SOS of pressure waves in solid materials, which are calculated by our SAM system, can be described by the following equation if the material is assumed to be isotropic:

$$c = \sqrt{E(1-\nu) / \rho(1+\nu)(1-2\nu)}, \quad (2)$$

where E is Young's modulus or the elastic modulus, ρ is the density, and ν is Poisson's ratio. This relationship shows that Young's modulus (the elastic modulus) of the tissue and the SOS are closely related [10].

3. Preparation of sample materials

Fresh frozen or formalin-fixed, paraffin-embedded sections are cut flat to a thickness of 10 μm and used to obtain observations. Excessively thin samples are not suitable for acquiring correct measurements. Excessively thick samples ($>20 \mu\text{m}$) are not suitable for detecting the returned waves due to the loss of energy. In addition, samples with irregular surfaces will scatter sound and hinder observations.

A cytology specimen is prepared as a single cell layer on a slide using a liquid-based cytology method (BD CytoRichTM; Franklin Lakes, NJ, USA). This method can be used to collect cells on the slide by ionic binding. Because the cells are negatively charged, they spontaneously bind to the slide, which has a positive charge [8].

4. Observation procedure of SAM

The SAM (AMS-50SI) system employed in our studies was manufactured by Honda Electronics (Toyohashi, Aichi, Japan), and it was equipped with a 120-MHz (resolution = approximately 13 μm) or 320-MHz (resolution = 4.7 μm) transducer. The SAM images of an object were obtained by plotting the SOS through the sections on the screen.

To perform SAM imaging, the slide sections were placed upside down on the stage above the transducer, and distilled water was applied between the transducer and the section as a coupling fluid because air interferes with sound transmission. After mechanical X-Y scanning, the SOS was calculated from each point on the section and plotted on the screen to create two-dimensional, color-coded images. The vertical bar on the left and the horizontal bar at the bottom of each figure indicate the distance (mm) on the slide. The vertical colored column on the right side of the figure indicates the average SOS of each square area on the section. The color range of observation can be changed manually. The region of interest (0.3, 0.6, 1.2, 2.4, or 4.8 mm^2) employed for acoustic microscopy was determined based on light microscopic (LM) images. The SOS values were calculated at 300×300 points and plotted on the screen to create the images, and sound data from 64 cross points on the lattice screen were used for statistical analysis. Other data such as the thickness of the section and AOS were also obtained from each point and shown on the screen.

5. Application of SAM to tissue and cytology diagnosis

In general, pathologists use LM images of sections for histological diagnosis. However, SAM can provide additional or novel information about the same section without staining and within a few minutes. Several examples are described as follows:

5.1. Skin

Changes associated with aging and environmental factors are apparent in the skin [11, 12]. These characteristic changes include thinning of the epidermis with a flattened dermal-epidermal junction, decreased amounts of collagen, elastin, ground substance, and eccrine/apocrine glands in the dermis, and the presence of solar elastosis in the upper dermis of sun-damaged skin.

Figure 3 compares SOS images of the facial skin in elderly and juvenile subjects. The SOS values for the epidermis are greater in the elderly subject than in the juvenile subject, which may indicate the loss of water in the dry skin of the elderly subject compared with the moist skin

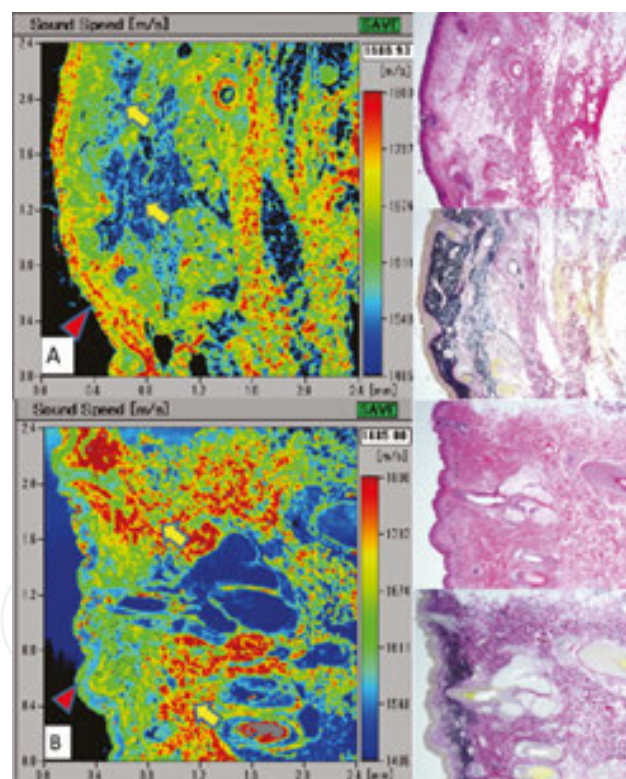


Figure 3. Comparative skin images of SOS in juvenile and elderly subjects. The skin of the elderly subject (A) has higher and lower SOS values in the epidermis (arrow head) and superficial dermis (arrows), respectively. By contrast, the skin of the juvenile subject (B) has lower and higher SOS values in the epidermis (arrow heads) and dermis (arrows), respectively. In the skin of the elderly subject, elastic fibers are diffusely deposited under the epidermis due to solar elastosis, whereas thick collagen fibers are distributed between the skin adnexa of the superficial dermis in the skin of the juvenile subject. The corresponding LM images with hematoxylin and eosin (right upper) and elastica-van-Gieson (right lower) staining are shown.

of the juvenile subject. The dermal low SOS areas in the elderly subject correspond to solar elastosis, which can be seen as black fibrillary materials by elastic-van-Gieson staining, whereas the dermal high SOS areas in the juvenile subject are consistent with collagen-rich contents. Thus, SAM can provide structural and biochemical information.

5.2. Artery

Narrowing (stenosis) and weakening are the two principle mechanisms of vascular disease [13]. The renal arteries (RAs) of elderly (101-year-old female) and young (30-year-old male) subjects are compared in **Figure 4**. The young subject's RA has a three-layer structure, that is, intima, media, and externa, with uniform thickness and SOS values, respectively. By contrast,

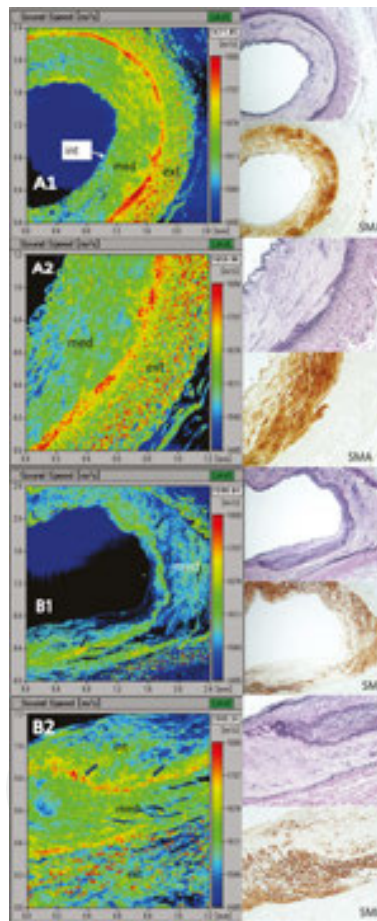


Figure 4. SOS images of the renal arteries in (RAs) young (A) and elderly (B) subjects. The RA has a three-layered structure, that is, intima, media, and externa with elastic laminae between each layer. The RA of a young subject (A1, A2) has a regular-layered structure, whereas that of an elderly subject (B1, B2) has an irregular shape and thickness. The thick intima with atheroma deposition has a low SOS value. The broad internal elastic lamina (arrows) has higher SOS values than those of the intima and media. The tunica media with variable thickness comprises smooth muscle fibers, which partly disappear with age. The externa comprises thick collagen fibers, which are lower in number in elderly subjects compared with young subjects. The corresponding LM images with elastica-van-Gieson staining and anti-smooth muscle immunostaining (SMA) are shown on the right. ext, externa; int, intima; med, media.

the elderly subject's RA has lost the layered structure with an irregular inner lumen. A thick intima with atheroma (lipids) deposition yields low SOS values. A broad intimal elastic lamina produces higher SOS values than the intima and media. The media with variable thickness comprises smooth muscle fibers that have partly disappeared. The externa has a decreased number of thick collagen fibers, which are clearly visible in the SOS image.

Therefore, SAM performs better than LM by simultaneously displaying structural changes and functional changes indicative of weakening.

5.3. Cardiac valve

Aortic valves (AVs) have a three-layered structure, that is, fibrosa, spongiosa, and ventricularis, as shown in **Figure 5**. The AVs of a young patient possess this layered structure with uniform high, middle, and lowest SOS values for the fibrosa, ventricularis, and spongiosa layers, respectively. By contrast, the elderly patient exhibits changes due to aging such as

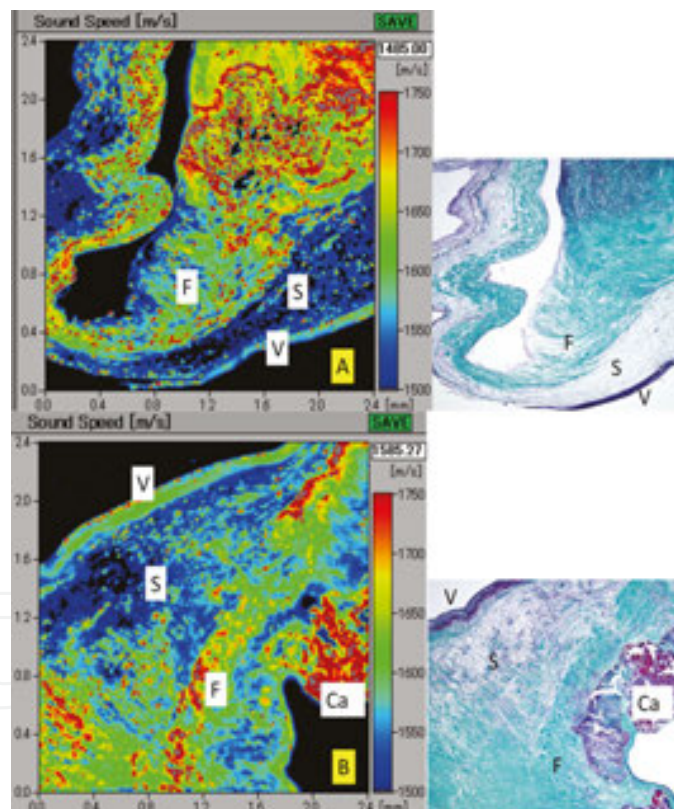


Figure 5. SOS images of aortic valves (AVs) in young (A) and elderly (B) patients. AVs have a three-layered structure, that is, fibrosa, spongiosa, and ventricularis. The AV of young patients has this layered structure, where the fibrosa, ventricularis, and spongiosa have high, middle, and low SOS values, respectively. The elderly patient exhibits changes in the AV due to aging such as nodular calcification. The SOS image shows that the highest values indicate calcification. The fibrosa has variable thickness and SOS values. The collagen bundles crumble in some places with age. Some collagen fibers drop into the spongiosa, and their interface is vague. The corresponding LM image with elastica-Masson staining is shown on the right. F, fibrosa; Ca; calcification; S, spongiosa; V, ventricularis.

nodular calcification. The SOS image assigns the greatest values to calcification. The fibrosa has a variable thickness and SOS values. The collagen bundles have crumbled in places to form vague interfaces.

Figure 6 shows the AV of a subject with Marfan's syndrome, who needs replacement therapy due to weakening, where the ventricularis is thickened, and fibronectin has accumulated. The SAM image contains variable SOS values at the ventricularis and uneven high SOS values at the fibrosa where disorganized fiber arrays can be seen.

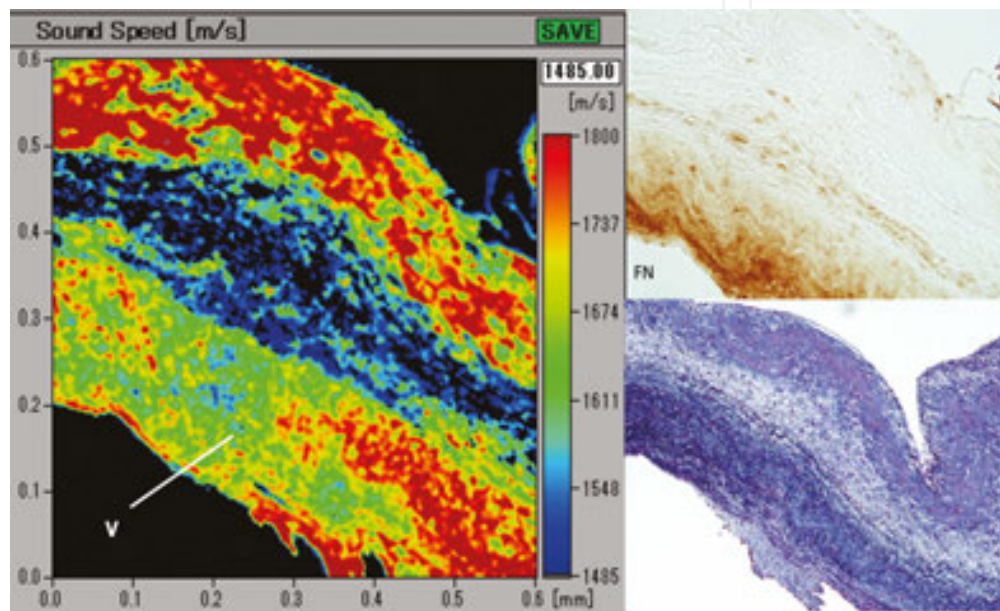


Figure 6. SOS image of the aortic valve in a subject with Marfan's syndrome. The ventricular layer is rich in thick elastic fibers with irregular SOS values. The fibrosa layer is rich in collagen fibers with uneven SOS values and disorganized fiber arrays. The corresponding LM images with elastica-Masson staining and anti-fibronectin immunostaining are shown on the right. V, ventricularis.

The SAM image can visualize collagen and elastin fiber abnormalities both morphologically as well as functionally according to the SOS values.

5.4. Gastrointestinal tract

The gastrointestinal tract basically comprises five layered structures, that is, mucosa, submucosa, muscularis propria, subserosa, and serosa. SAM images can be used to discriminate these layered structures (**Figure 7A**). In cancer, these regular structures are disturbed by cancer invasion (**Figure 7B**). The invaded areas can be detected based on changes in both the morphology and the SOS values.

A carcinoma and a benign adenoma in colon polypectomy are shown in **Figure 8**, where there is an irregular tubular structure with variable high SOS values in the cancer compared with the adenoma.

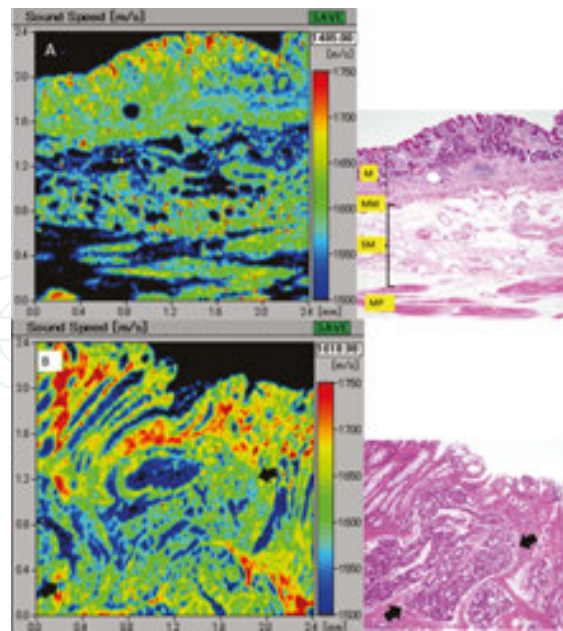


Figure 7. SAM image of normal stomach and gastric adenocarcinoma. From top to bottom, the normal gastric wall (A) comprising the mucosa, muscularis mucosae (MM), submucosa (SM), and muscularis propria (MP). A gastric tubular carcinoma (B) can be seen invading the normal mucosa (arrows). The stroma in the vicinity of the cancer nest has a higher SOS value than the cancer cells. The corresponding LM images with hematoxylin and eosin staining are shown on the right.

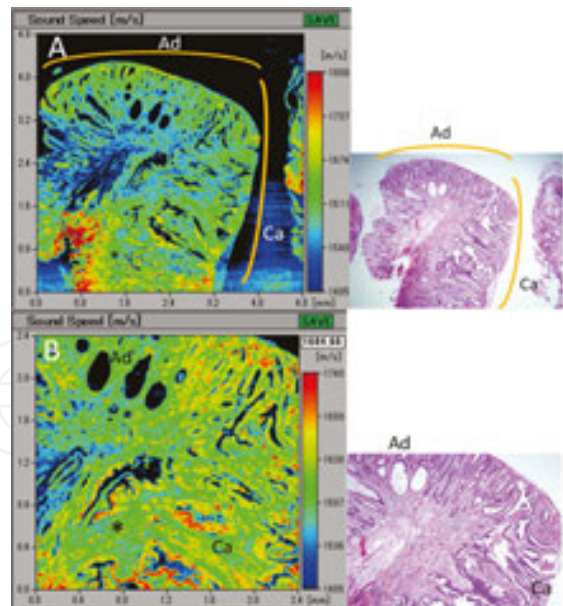


Figure 8. SOS images of adenocarcinoma in tubular adenoma. A colon polypectomy specimen is shown, which contains an adenocarcinoma region in a tubular adenoma (A, low magnification; B, high magnification). The adenoma comprises regular tubular structures, whereas the carcinoma is made of irregular branched tubules. The SOS image of carcinoma has irregular high values, and the shapes of the tubules are more variable compared with the adenoma. The stroma of the carcinoma at the invasive site (*) has a higher SOS value than the adenoma. The corresponding LM images with hematoxylin and eosin staining are shown on the right. Ad, adenoma; Ca, carcinoma.

5.5. Placenta

A placenta is rich in blood vessels where the exchange of gases and nutrients occurs between the maternal and fetal circulations. Chorionic villi form a delicate mesh in the central stroma surrounded by trophoblasts, which can be visualized well by SAM (**Figure 9**). During inflammation, the villi have increased numbers of blood vessels and inflammatory cells, which can be clearly discriminated using SAM imaging.

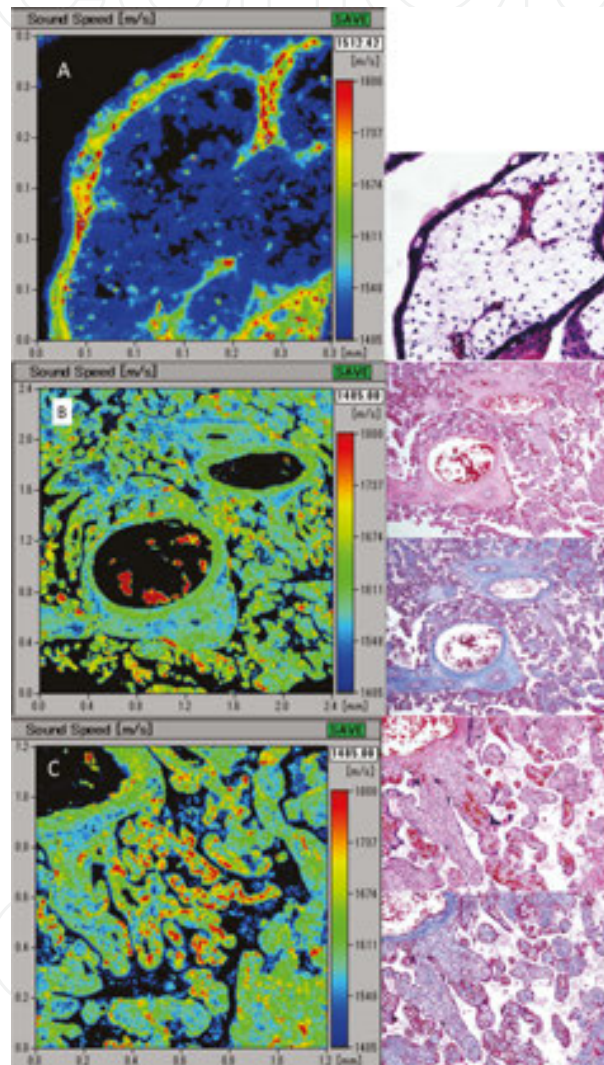


Figure 9. SOS image of placenta. Chorionic villi in the first trimester (A), where the central edematous stroma surrounded by trophoblasts is clearly visible. Erythroblasts in the vessels and trophoblasts have high SOS values. The nuclei of macrophages in the central stroma are visible as dot-like higher SOS spots. The third-trimester chorionic villi have chronic villitis (B, low magnification; C, high magnification) with hypervascular stroma and lymphocytic infiltration. The congested villi with anastomotic capillaries have high SOS values. The corresponding LM images with hematoxylin and eosin staining and Masson trichrome staining are shown on the right.

The blood contents produce very high SOS values, so it is easy to detect changes in the number and size of blood vessels.

5.6. Liver and lung

According to SAM observations, fibrosis comprises collagen fibers with high SOS values. Liver cirrhosis (**Figure 10A**) and pulmonary fibrosis (**Figure 10B**) are representative lesions due to fibrosis. More severe fibrosis yields greater SOS values, and thus the degree of fibrosis can be compared among lesions.

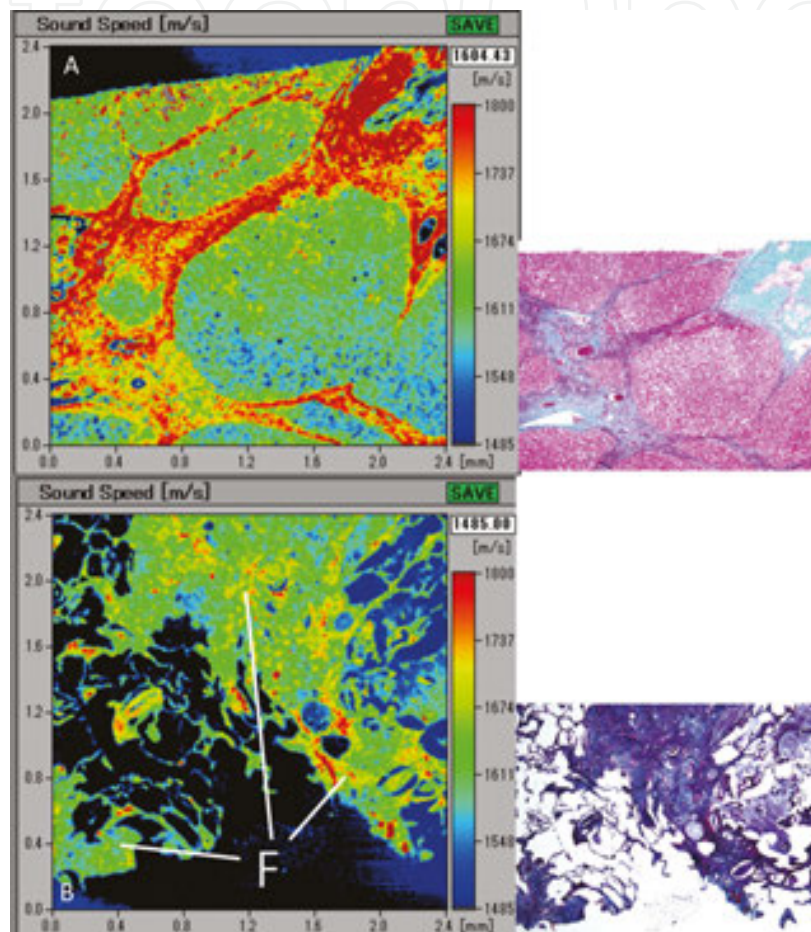


Figure 10. SOS images of liver cirrhosis and pulmonary fibrosis. Liver cirrhosis (**A**) and pulmonary fibrosis (**B**) are representative lesions with fibrosis. In liver cirrhosis, fibrosis with high SOS values surrounds pseudolobules. In pulmonary fibrosis, areas with interstitial fibrosis have high SOS values in the lung. The corresponding LM images with Masson trichrome staining are shown on the right. F, fibrosis.

5.7. Kidney

In diabetes mellitus, the kidney exhibits nodular glomerular sclerosis, and the tubules have thickened basement membranes (**Figure 11**). According to SOS imaging, a sclerotic portion of the glomerulus and tubular basement membranes surrounding the tubular lumen has greater SOS values compared with other glomerular and tubular areas. The SAM imaging system provides digital SOS data, which facilitates comparisons of the severity of sclerosis and elasticity among lesions and cases.

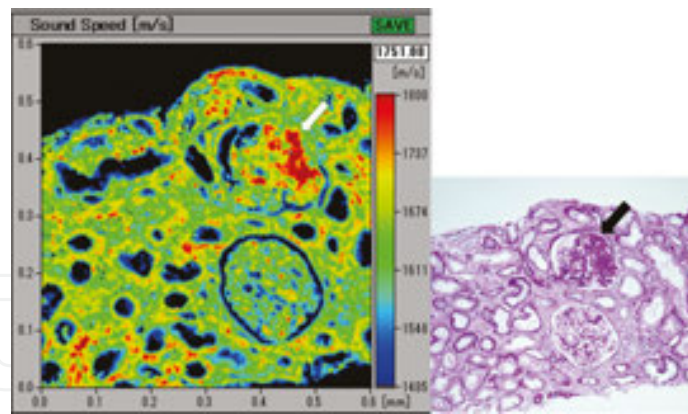


Figure 11. SOS image of diabetes mellitus kidney patient. The kidney of a diabetes mellitus patient has nodular sclerosis of the glomerulus and thickening of the basement membrane. According to SOS imaging, a sclerotic region of the glomerulus (arrow) has a higher SOS value compared with other glomerular areas. Tubular basement membranes surrounding the tubular lumen also have higher SOS values. The corresponding LM image with periodic acid-Schiff staining is shown on the right.

5.8. Heart

Acute myocardial infarction is sometimes difficult to detect in the areas involved. However, SOS images of coagulative necrosis indicate crumbled cardiac muscles with greater SOS values compared with the intact muscles (**Figure 12**). The elasticity of the necrotic area changes during the time course of infarction, and the SOS images may change accordingly.

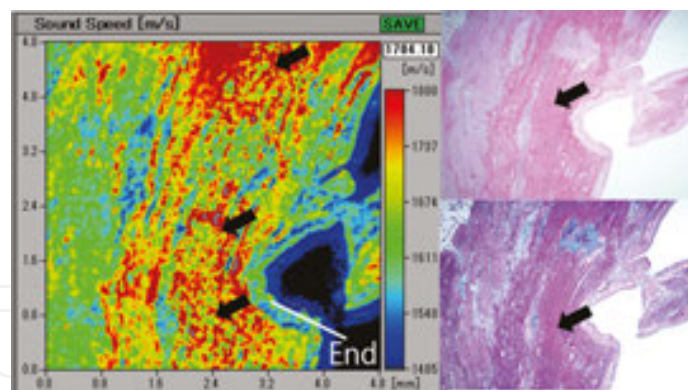


Figure 12. SOS image of acute myocardial infarction. An area with acute infarction and coagulative necrosis contains crumbled cardiac muscles (arrows). The necrotic areas have higher SOS values than intact cardiac muscles on the more endocardial side. The corresponding LM images with hematoxylin and eosin and Masson trichrome staining are shown on the right. End, endocardium.

5.9. Thyroid

Papillary carcinomas are the most common carcinoma in the thyroid. Their typical histology comprises papillary structures with thin elongating and branching cores. The SOS images (**Figure 13**) are comparable with optical images. Compressed follicles and fibrous stroma in

the invasive sites have very high SOS values, where any abnormalities make it easy to detect cancer.

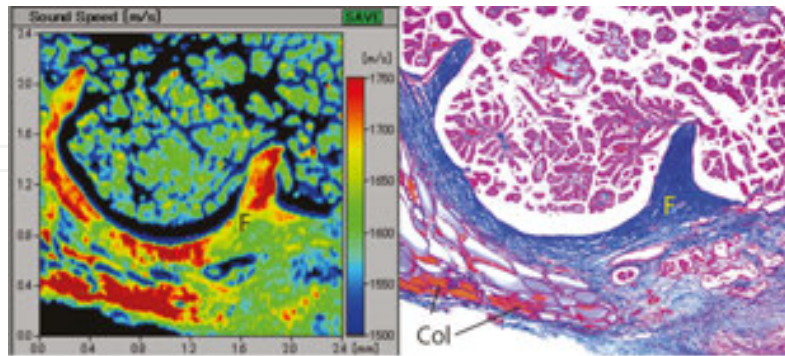


Figure 13. SOS image of papillary carcinoma of the thyroid. A papillary carcinoma comprises thin elongating branching cores with uniform low SOS values compared with the surrounding fibrous stroma (F). Compressed thyroid follicles have high SOS values due to their colloid contents (Col). The corresponding LM image with Masson trichrome staining is shown on the right.

Hashimoto's thyroiditis (or chronic lymphocytic thyroiditis) is characterized by many lymphoid follicles among the thyroid follicles (**Figure 14**). The lymphoid follicles have low SOS values in the thyroid. The SOS values of colloids vary according to their concentration, and a high concentration of colloids is seen in a low functioning thyroid; thus, SOS imaging may be used to predict the thyroid activity.

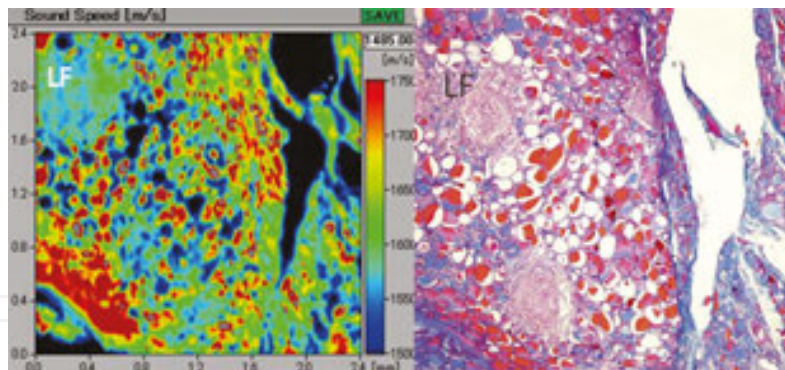


Figure 14. SOS image of Hashimoto's thyroiditis. The concentrated colloids in the thyroid follicles have high SOS values compared with the patchy lymph follicles (LF). The corresponding LM image with Masson trichrome staining is shown on the right.

5.10. Cytology

Differentiating malignant and benign cells in body fluids is possible using SAM [8]. Malignant cells have higher SOS values and irregular shapes compared with benign cells.

In urine cytology, cells with larger sizes and irregular shapes correspond to urothelial carcinoma cells, most of which have high SOS values (**Figure 15A**).

Among brain tumors, glioblastomas are the most common malignant tumor, and the cells have an irregular spindle shape with variable size (**Figure 15B**), where they are connected with each other. These features are characteristic of malignant brain gliomas.

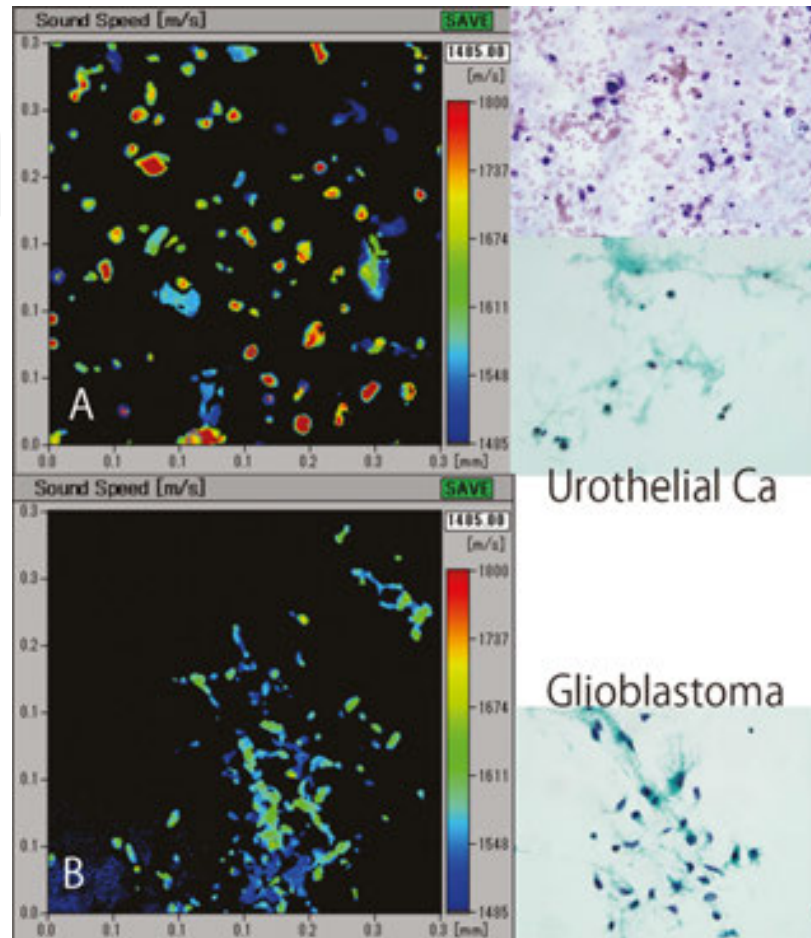


Figure 15. SOS image of urothelial carcinoma and glioblastoma. Cells with various different shapes and sizes are present in the urine. Large cells with irregular shapes correspond to urothelial carcinoma cells, most of which are shown in red in the SOS image (A). A touch smear of a brain tumor was obtained by SAM (B). Irregular spindle-shaped cells are connected to each other, and the size and shape of the cells vary. LM images with Giemsa or Papanicolaou staining obtained using the same specimen are shown on the right.

The thin preparation method in cytology (<http://www.bdj.com/jps/brush>) can be employed to assemble cells in a single cell layer at the center of a slide. Each cell or cell cluster is separate, which makes it easy to find cancer cells. SAM is a useful tool for screening cells without the necessity for staining.

6. Differentiation between malignant and benign effusions

When malignant and benign effusions are compared, the former have higher SOS values than the latter, but there is no significant difference in the mean thicknesses of the two cell types.

The original SOS image can be converted into a bipolar image comprising up and down cutoff point values. By adjusting the observation range, the malignant cells can be readily differentiated from benign cells (**Figure 16**).

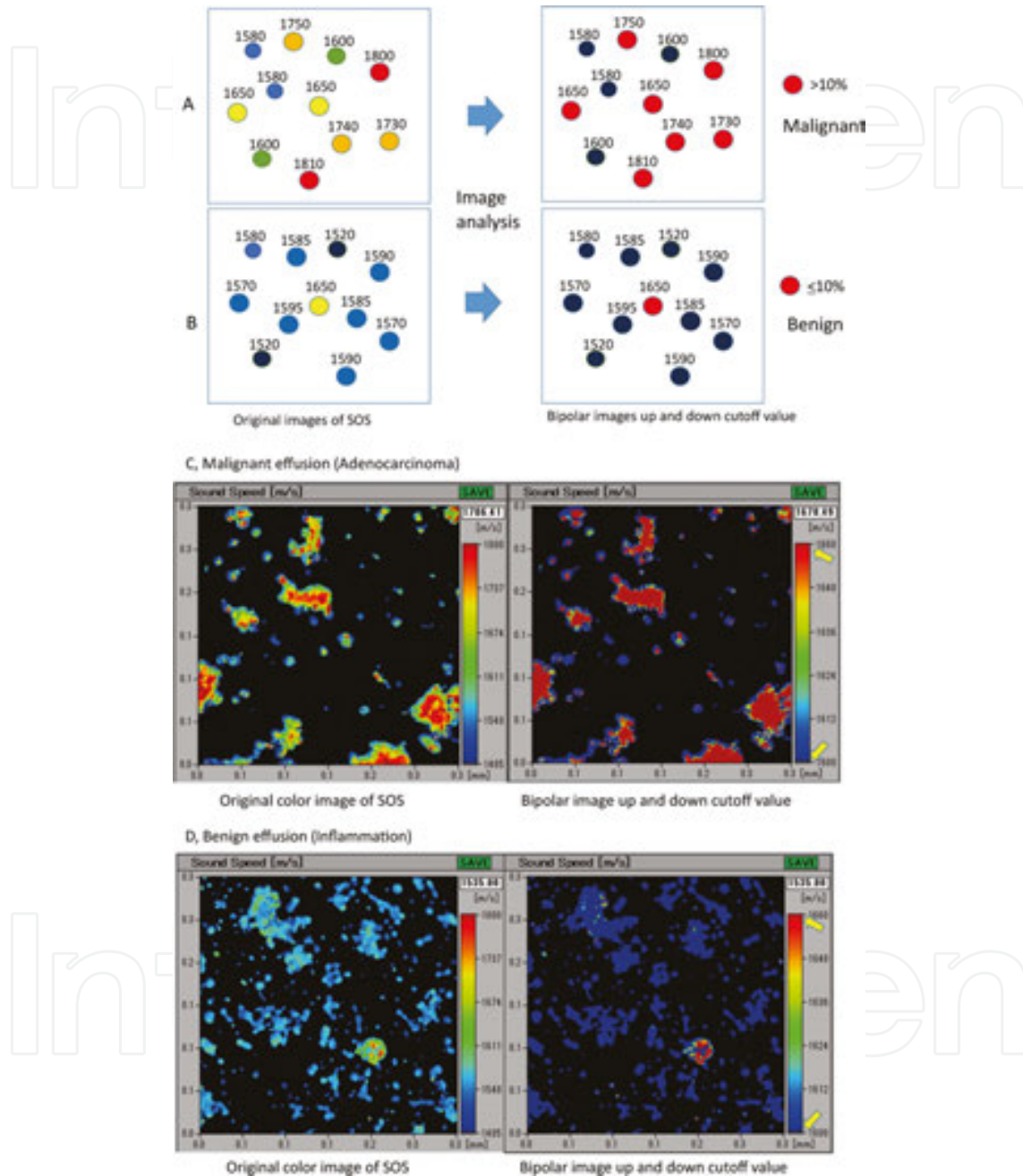


Figure 16. Differentiating benign and malignant effusions. **A** (malignant) and **B** (benign) show schematic color images obtained by SAM, where the SOS values are shown in the cells. These images were converted into bipolar red and blue images using up and down cutoff point values. If more than 10% of the single cells or small clusters had values higher than the cutoff point, they were regarded as a malignant effusion in SAM. Real SOS images of malignant (**C**) and benign (**D**) effusions are shown on the left. The bipolar images on the right were obtained based on the up and down cutoff point values. These images were obtained by limiting the range of the color scale bar on the right-hand side of the screen (yellow arrows).

7. SOS changes by fixation

The two main types of cross-linking and noncross-linking fixatives are formalin and ethanol, respectively. Changes in the SOS values have been reported after formalin fixation [6]. The differences in the SOS values and thickness were also compared using formalin and ethanol fixation. Using tannic acid fixation, the SOS values increase according to the concentration and duration of fixation (**Figure 17**).

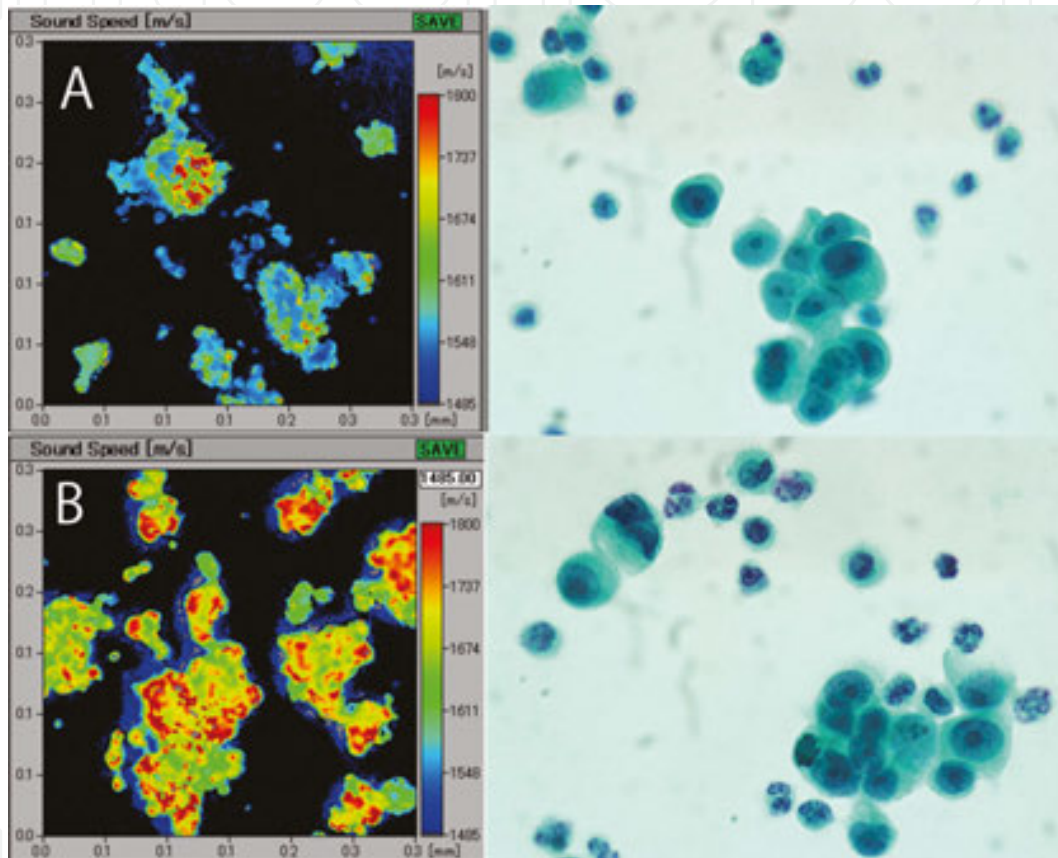


Figure 17. Effects of tannic acid fixation on cytology specimens. A cytological slide with an adenocarcinoma specimen was fixed in 1% tannic acid for 10 min. The SOS images obtained before (**A**) and after (**B**) fixation are compared. After fixation, the SOS values increased in the adenocarcinoma, which indicates that the cells became harder. The outer contour became clearer, and thus it was easier to detect the large cells/clusters as well as the irregular high SOS values. The corresponding LM image with Papanicolaou staining is shown on the right.

8. Effects of PAS reaction on SOS imaging

After the PAS reaction, the SOS values increase according to the strength of optical staining (**Figure 18**), where the more glycosylated regions appear as higher SOS areas. The degree of glycosylation may be evaluated objectively to allow comparisons among lesions and cases.

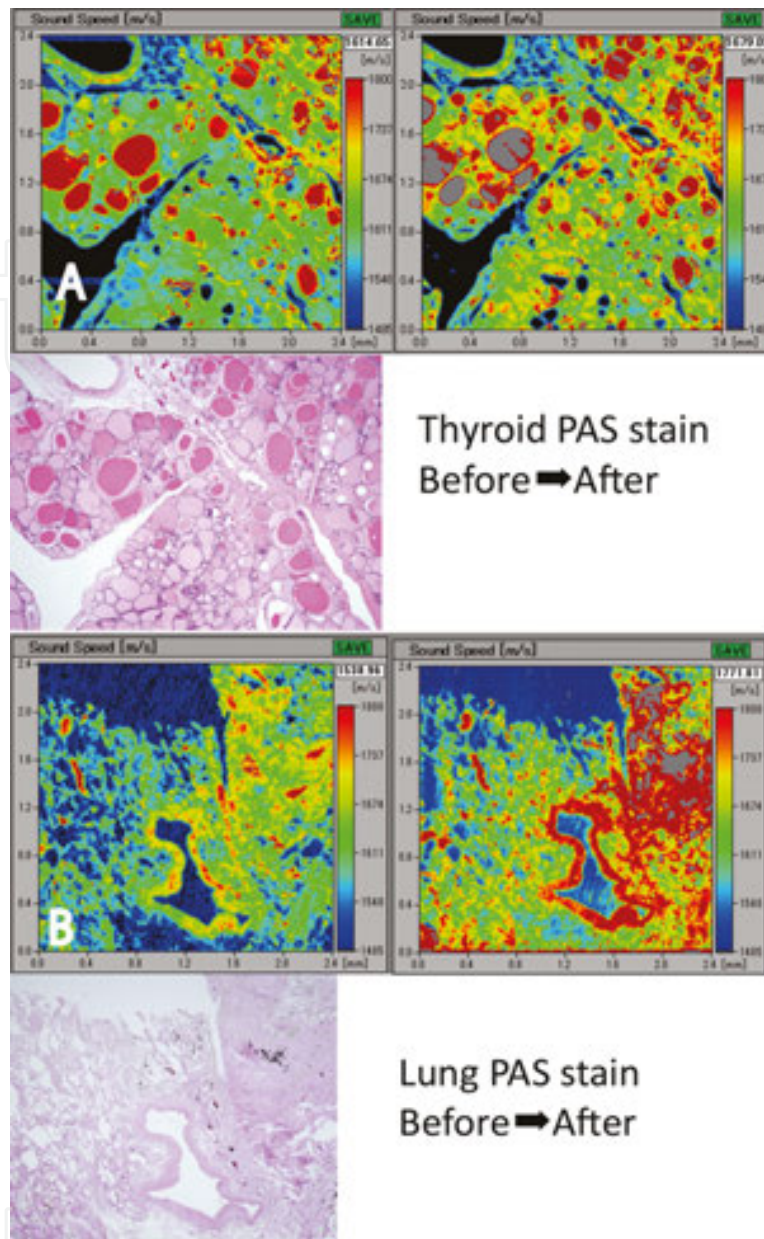


Figure 18. Effects of periodic acid-Schiff staining on SOS images. The SOS values increased according to the intensity of periodic acid-Schiff staining. In a thyroid sample (A), the colloids in the thyroid follicles have high SOS values, where the intensity correlates with the concentration of the colloids. A lung sample (B) has high SOS values in the fibrosis and vascular walls.

9. Effects of collagenase on SOS values

Fibrosis is a consequence of inflammation, ischemia, cancer invasion, and other pathological events. Myofibroblasts produce collagen fibers that undergo chemical modifications such as glycation and bridging, where the degree of modification varies among tissues or with age. Younger collagen fibers without modification may appear in granulation tissues, and they are

vulnerable to protease digestion (**Figure 19A**). By contrast, the fibrous scar tissue seen in old myocardial infarctions (**Figure 19B**) resists protease breakdown because the chemical modifications interfere with the activity of protease.

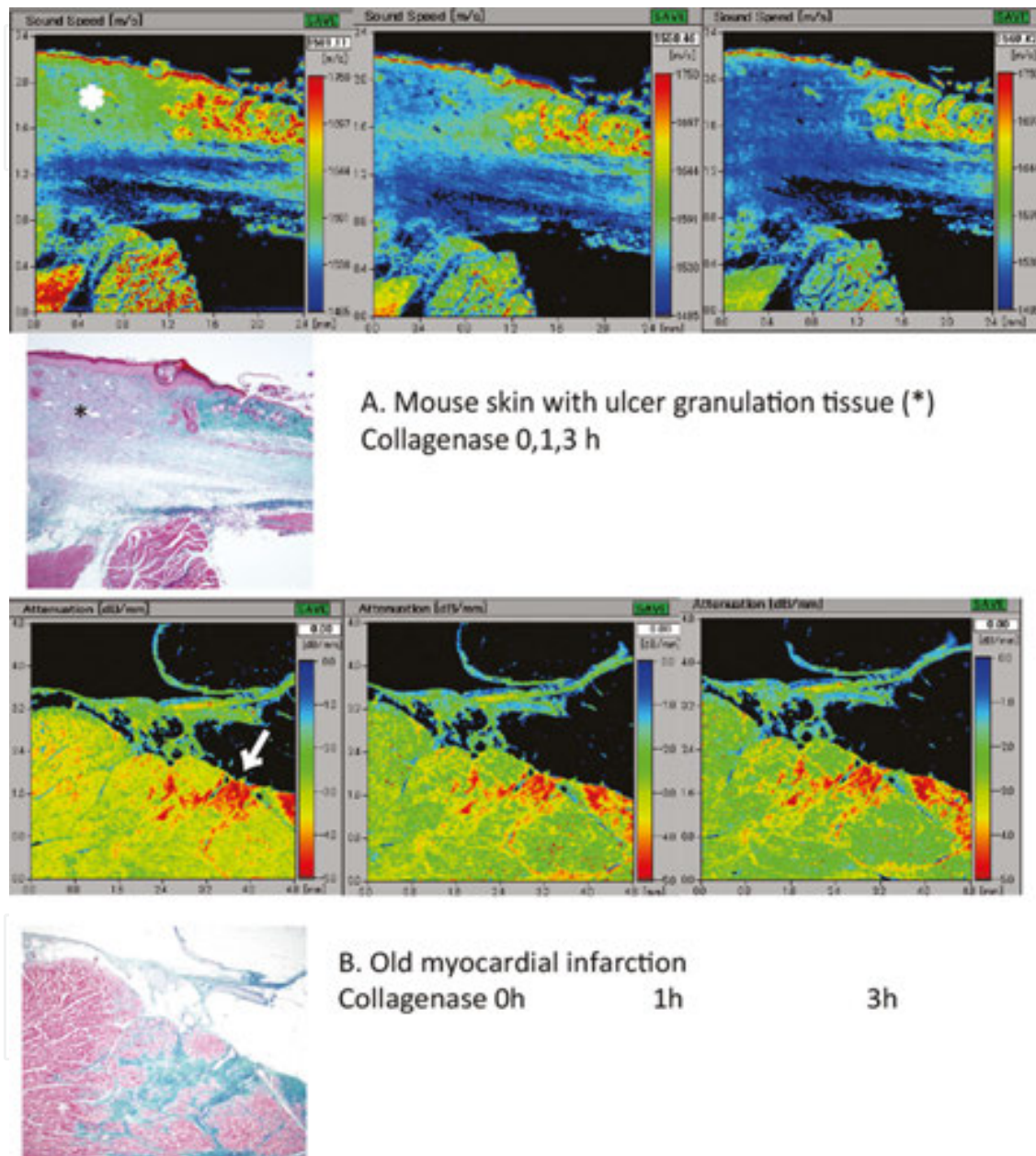


Figure 19. Effects of collagenase on SOS values. Changes in the SOS values in a section after collagenase treatment are shown. A newly formed fibrosis in granulation tissues in a skin ulcer (**A**) is vulnerable to collagenase digestion, whereas the old fibrous scar tissues (arrow) due to myocardial infarction (**B**) is resistant to the enzyme. The SOS values for the background epidermis and smooth muscles in **A** and the cardiac muscles in **B** decrease gradually.

The susceptibility to collagenases is also influenced by aging, where the dermal collagens in juvenile skin (**Figure 20A**) are digested more easily than those in elderly skin (**Figure 20B**).

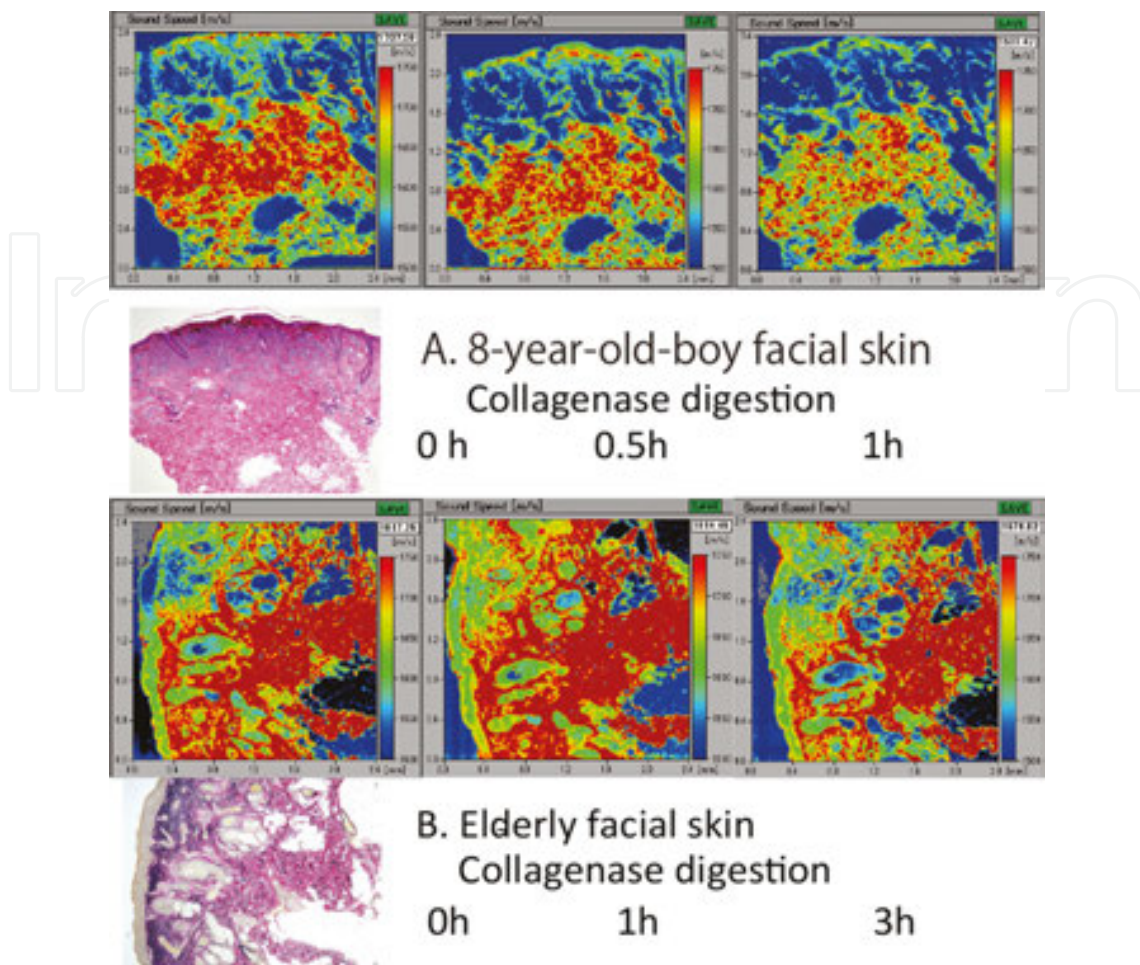


Figure 20. Differences in the susceptibility of juvenile and elderly skin to collagenases. The SOS values after collagenase digestion of the sections are compared in juvenile (A) and elderly (B) skin. The dermal SOS values of the juvenile skin decreased gradually, whereas those of the elderly skin were stable.

10. Statistical analysis of SOS

The SOS data obtained from each image were expressed as the mean and standard deviation (SD; m/s). Before the statistical tests mentioned below, normal distribution was confirmed using the test for difference of mean. One-way analysis of variance (ANOVA) was used to evaluate the SOS values. Significant differences were evaluated using multiple comparisons with the Tukey–Kramer’s test, with $P < 0.05$ considered statistically significant.

The mean and SD SOS values for squamous cell carcinomas, adenocarcinomas, mesotheliomas, lymphomas, and inflammatory cells in fluid are summarized in **Figure 21** and **Table 1**. Each cell type has a characteristic SOS value, and there are statistically significant differences ($P < 0.01$) between malignant and benign cells, as well as between epithelial cells and free cells in the blood. In general, malignant and epithelial cells have higher SOS values than benign cells and free cells in the blood, respectively.

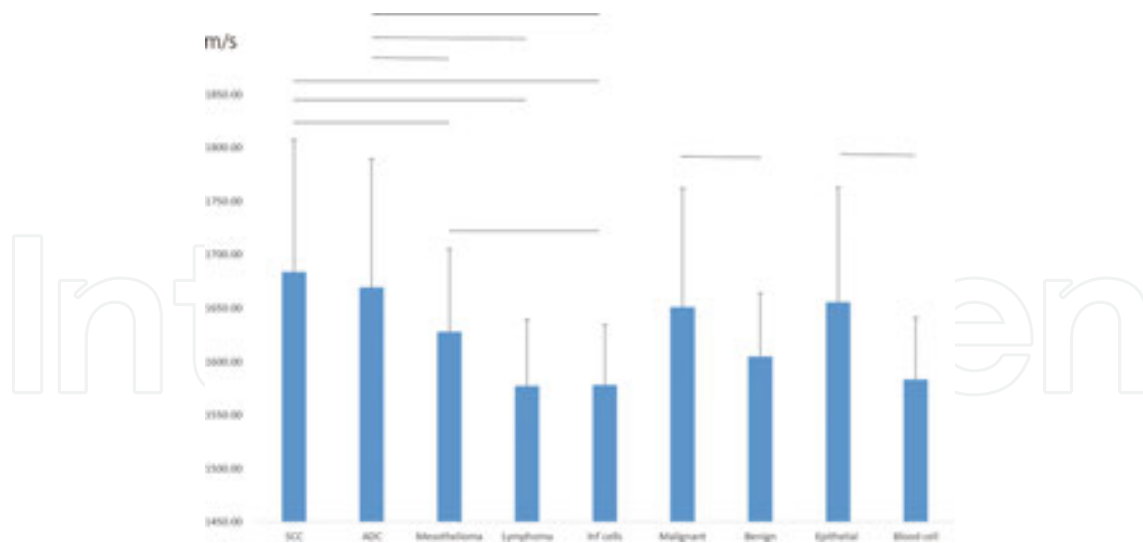


Figure 21. Mean and SD of SOS values among various cells in fluids. There SOS values differ significantly among cell types. The malignant cell group has significantly greater SOS values than the benign cell group ($P < 0.01$), and the epithelial group has higher SOS values than the blood cell group ($P < 0.01$). ADC, adenocarcinoma; Inf cell, inflammatory cells; SCC, squamous cell carcinoma.

Cell types	SOS AVE (m/s)	SD	<i>n</i>
SCC	1684.10	123.46	111
ADC	1669.61	120.10	356
Mesothelioma	1627.94	77.47	132
Lymphoma	1577.56	61.55	85
Inf cells	1578.38	56.23	81
Malignant	1651.10	110.99	711
Benign	1604.95	59.09	211
Epithelial	1655.69	107.31	729
Blood cell	1583.30	57.85	193

Table 1. Acoustic values of speed of sound among different cells in fluid. SCC, squamous cell carcinoma; ADC, adenocarcinoma; Inf cell, inflammatory cells.

In tissue sections, each tissue component has a specific SOS value, as shown in **Figure 22** and **Table 2** for the gastric walls, where the mucosal layers have lower SOS values than the muscularis mucosae or muscularis propria layers. Neoplasms usually have similar SOS values to their original tissues. Carcinomas arising from mucosal epithelia have almost the same SOS values as the mucosal layer, but poorly differentiated carcinomas have higher SOS values due to their desmoplastic reactions. Malignant lymphomas comprising free cells in the blood have low SOS values, as found with fluid cytology.

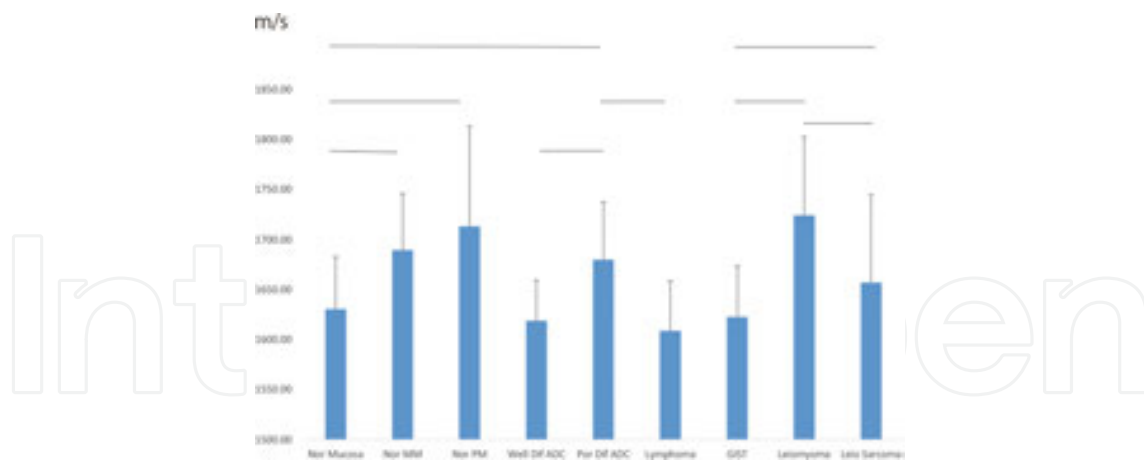


Figure 22. Acoustic values of SOS among gastric tissues. Comparison of the mean \pm SD of the SOS values among gastric tissues. There are statistically significant differences among different tissue components ($P < 0.01$). GIST, gastrointestinal stromal tumor; leio sarcoma, leiomyosarcoma; nor MM, normal muscularis mucosae; nor mucosa, normal mucosa; nor PM, normal muscularis propria; Por Dif ADC, poorly differentiated adenocarcinoma; Well Dif ADC, well-differentiated adenocarcinoma.

Gastric tissues	SOS Ave(m/s)	SD	<i>n</i>
Nor mucosa	1630.51	52.14	105
Nor MM	1689.47	56.43	57
Nor PM	1713.34	99.97	90
Well Dif ADC	1618.89	40.32	155
Por Dif ADC	1680.05	57.52	210
Lymphoma	1608.93	49.87	196
GIST	1622.96	50.18	171
Leiomyoma	1724.30	78.38	162
Leio sarcoma	1657.07	87.72	113

Nor Mucosa, normal mucosa, Nor MM, normal muscularis mucosae; Nor PM, normal muscularis propria; Well Dif ADC, well-differentiated adenocarcinoma; Por Dif ADC, poorly differentiated adenocarcinoma; GIST, gastrointestinal stromal tumor; Leio Sarcoma, leiomyosarcoma.

Table 2. Acoustic values of speed of sound among different gastric tissues.

11. Conclusion

SAM has five unique features compared with optical microscopy. First, the measurement procedure is rapid and easy, without any requirement for special staining. The magnification of the images can be changed simply by selecting the area for scanning. Second, the observation ranges of SOS are adjustable, which facilitates the detection of specific cells such as malignant cells. Third, observations are repeatable under different conditions using the same slide so time course observations may be obtained before and after events. Fourth, the microscopic acoustic properties correspond to the echo intensity and texture in clinical echography. Finally,

SAM data can help to assess the biomechanical characteristics of tissues and cells, such as elasticity, to statistically compare their digital values [14].

However, there are some limitations of this technique. First, appropriate sample preparations are necessary such as flat 10- μm sections or single-layered cytology samples. Second, observation areas are limited. In our system, observation range is from $0.3 \times 0.3 \text{ mm}^2$ to $4.8 \times 4.8 \text{ mm}^2$ at the maximum. We usually refer to LM image to determine the observation area of SAM. Third, discrimination between nuclei and cytoplasm of the cell is so difficult that we can obtain only cell contours.

For overcoming the current limitations, new technologies are been developed. The wavelength of ultrasound can be shorter than that of visible light, so the resolution of ultrasound overcomes that of the LM to facilitate the observation of organelles in cells. New transducers with much shorter wave lengths are been developed. For observing living cells, impedance mode of SAM observation without contact with cells is on the way [15]. For making contrast images to specify particular structures, new techniques are necessary. We are developing new acoustic staining or immunostaining with high SOS value materials. Acoustic images can illustrate different properties of tissues and cells compared with that by LM images. Developing new acoustic techniques may help to reveal more precise properties of tissues and cells in the future.

Acknowledgements

The author thanks T. Moriki and Y. Egawa for providing clinical samples and Y. Kawabata, N. Suzuki, and K. Sugaya for preparing the tissue sections. The author also thanks K. Kobayashi for his technical support and advice on SAM observation. This study was supported by the Japan Society for the Promotion of Science KAKENHI, Scientific Research Grant Number (c) 15K08375.

Author details

Katsutoshi Miura

Address all correspondence to: kmiura@hama-med.ac.jp

Division of Health Science, Hamamatsu University School of Medicine, Hamamatsu, Japan

References

- [1] Lemons RA, Quate CF. Acoustic microscopy: biomedical applications. *Science*. 1975;188(4191):905–11.

- [2] Briggs G, Kolosov O. Acoustic microscopy. Second edition. New York: Oxford University Press; 2010. 174–81 p.
- [3] Miura K, Yamamoto S. Pulmonary imaging with a scanning acoustic microscope discriminates speed-of-sound and shows structural characteristics of disease. *Lab Investig.* 2012;92(12):1760–5.
- [4] Miura K, Yamamoto S. Histological imaging of gastric tumors by scanning acoustic microscope. *Br J Appl Sci & Technol.* 2014;4(1):1–17.
- [5] Miura K, Mineta H. Histological evaluation of thyroid lesions using a scanning acoustic microscope. *Pathol Lab Med Int.* 2014;6:1–9.
- [6] Miura K, Egawa Y, Moriki T, Mineta H, Harada H, Baba S, et al. Microscopic observation of chemical modification in sections using scanning acoustic microscopy. *Pathol Int.* 2015;65(7):355–66.
- [7] Miura K, Nasu H, Yamamoto S. Scanning acoustic microscopy for characterization of neoplastic and inflammatory lesions of lymph nodes. *Sci Rep.* 2013;3:1255.
- [8] Miura K, Yamamoto S. A scanning acoustic microscope discriminates cancer cells in fluid. *Sci Rep.* 2015;5:15243.
- [9] Barr RJ, White GM, Jones JP, Shaw LB, Ross PA. Scanning acoustic microscopy of neoplastic and inflammatory cutaneous tissue specimens. *J Invest Dermatol.* 1991;96(1):38–42.
- [10] Saijo Y. Acoustic microscopy: latest developments and applications. *Imaging Med.* 2009;1(1):47–63.
- [11] Fenske NA, Lober CW. Structural and functional changes of normal aging skin. *J Am Acad Dermatol.* 1986;15(4 Pt 1):571–85.
- [12] Venazquez E, Murphy G. Histology of the skin. In: Elder D, Elenitsa R, Johnson B, Murphy G, Xu X, editors. *Histopathology of the skin.* Philadelphia, PA, USA: Lippincott Williams & Wilkins; 2009.
- [13] Mitchell RN. Blood vessels. In: Kumar V, Abbas AK, Aster JC, editors. *Pathologic basis of disease.* Philadelphia, PA: Elsevier; 2015. p. 483–522.
- [14] Saijo Y. Recent applications of acoustic microscopy for quantitative measurement of acoustic properties of soft tissues. In: Mamou J, Oelza ML, editors. *Quantitative ultrasound in soft tissues.* Heiderberg, Germany: Springer; 2013. p. 291–313.
- [15] Gunawan AI, Hozumi N, Takahashi K, Yoshida S, Saijo Y, Kobayashi K, et al. Numerical analysis of acoustic impedance microscope utilizing acoustic lens transducer to examine cultured cells. *Ultrasonics.* 2015;63:102–10.

